Supporting Information

High-Performance Supercapacitors Based on MnO_2 Tube-in-Tube Arrays

Xue-Feng Lu, An-Liang Wang, Han Xu, Xu-Jun He, Ye-Xiang Tong, and Gao-Ren Li*

MOE Laboratory of Bioinorganic and Synthetic Chemistry, KLGHEI of Environment and Energy Chemistry, School of Chemistry and Chemical Engineering, Sun Yat-sen University, Guangzhou 510275, China

Material characterization

The morphology and microstructure of the fabricated materials are characterized by field-emission scanning electronmicroscopy (FE-SEM, JSM-6330F), X-raydiffractometry (XRD, D8ADVANCE), transmission electron microscopy (TEM, Tecnai™ G2 F30). The chemical composition of the samples was characterized by energy-dispersive X-ray spectroscopy (EDS, INCA 300) and X-ray photoelectron spectroscopy (XPS, ESCALAB 250). All XPS spectra were corrected using the C 1s line at 284.6 eV. Inductively coupled plasmaatomic emission spectroscopy (ICP, SPECTRO) was used to analyze the loading of manganese dioxide. The mass loading of MnO_2 TTAs and STAs is 0.32 and 0.16 mg/cm^2, respectively.

Calculation methods of C_{sp}, power density and energy density

The specific capacitance (C_{sp}) determined from the cyclic voltammometric curves were calculated

according to Eqs. (1~2):

$$C_{\mathrm{sp}} = \frac{1}{A\Delta \mathrm{V}} \int_{\mathrm{y}}^{\mathrm{x}} i \mathrm{dt} \qquad (1)$$

$$C_{\mathrm{sp}} = \frac{1}{w\Delta \mathrm{V}} \int_{\mathrm{y}}^{\mathrm{x}} i \mathrm{dt} \qquad (2)$$

Where *i*, ΔV, *A* and *w* were the current (mA), voltage range of one scanning segment (V), electrode area (cm^2) and weight of the electrode material (mg), respectively.

The specific capacitance (Csp) determined from the chronopotentiometric curves were calculated according to Eqs. (3~4):

$$C_{\mathrm{sp}} = \frac{I\Delta \mathrm{t}}{\mathrm{A}\Delta \mathrm{V}} \qquad (3)$$

$$C_{\mathrm{sp}} = \frac{I\Delta \mathrm{t}}{\mathrm{w}\Delta \mathrm{V}} \qquad (4)$$

The energy density (*E*), and power density (*P*) were also calculated from the chronopotentiometric curves according to Eqs (5~6):

$$\mathrm{E} = \frac{1}{2} C_{\mathrm{sp}} (\Delta \mathrm{V})^2 \qquad (5)$$

$$\mathrm{P} = \frac{\mathrm{E}}{\Delta \mathrm{t}} \qquad (6)$$

Where *I* is the charge/discharge current, Δt is the time for a full charge ordischarge, *w* is the mass of the active electrode material, and ΔV is the voltage change after a full charge/discharge.

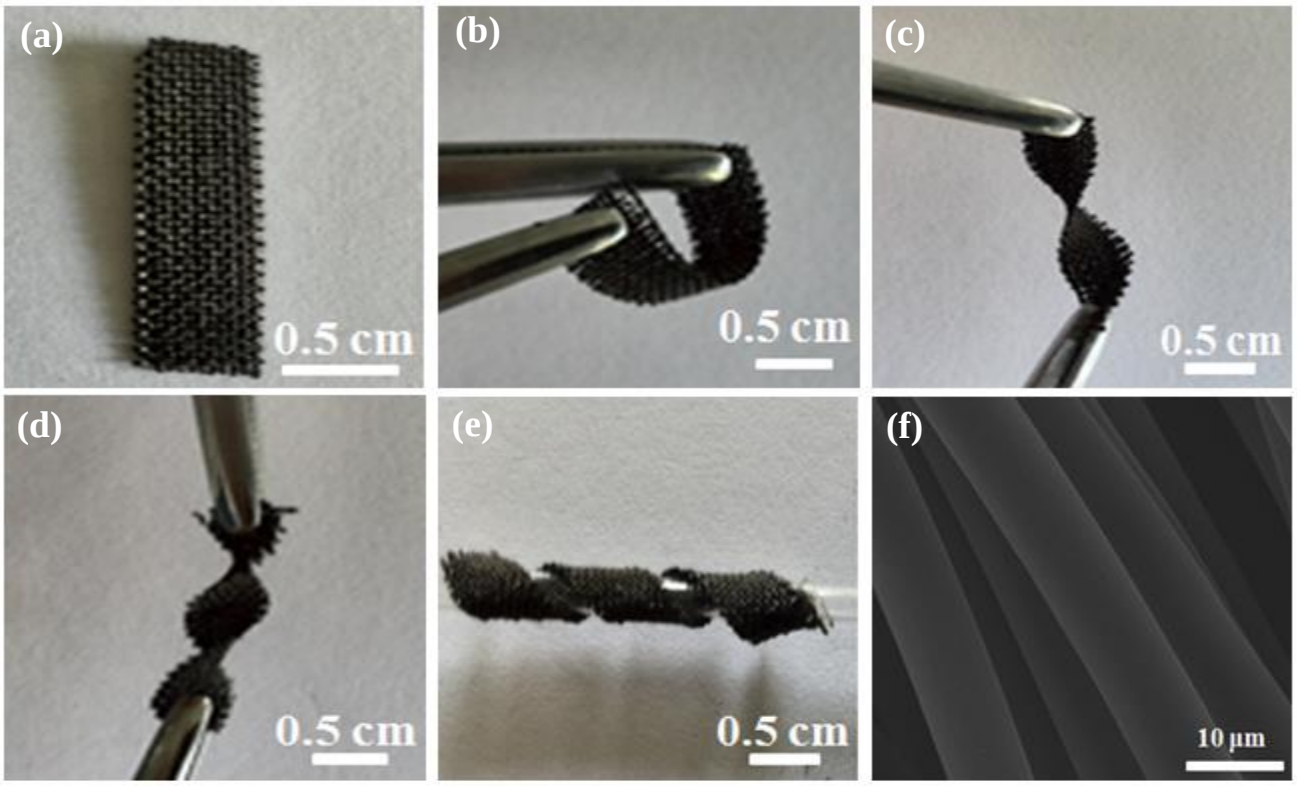

Figure S1. (a-e) Optical images of carbon fiber cloth (CFC) at normal states and various bending states, indicating the excellent flexible ability of the CFC; (f) Typical SEM image of carbon fibers in the CFC.

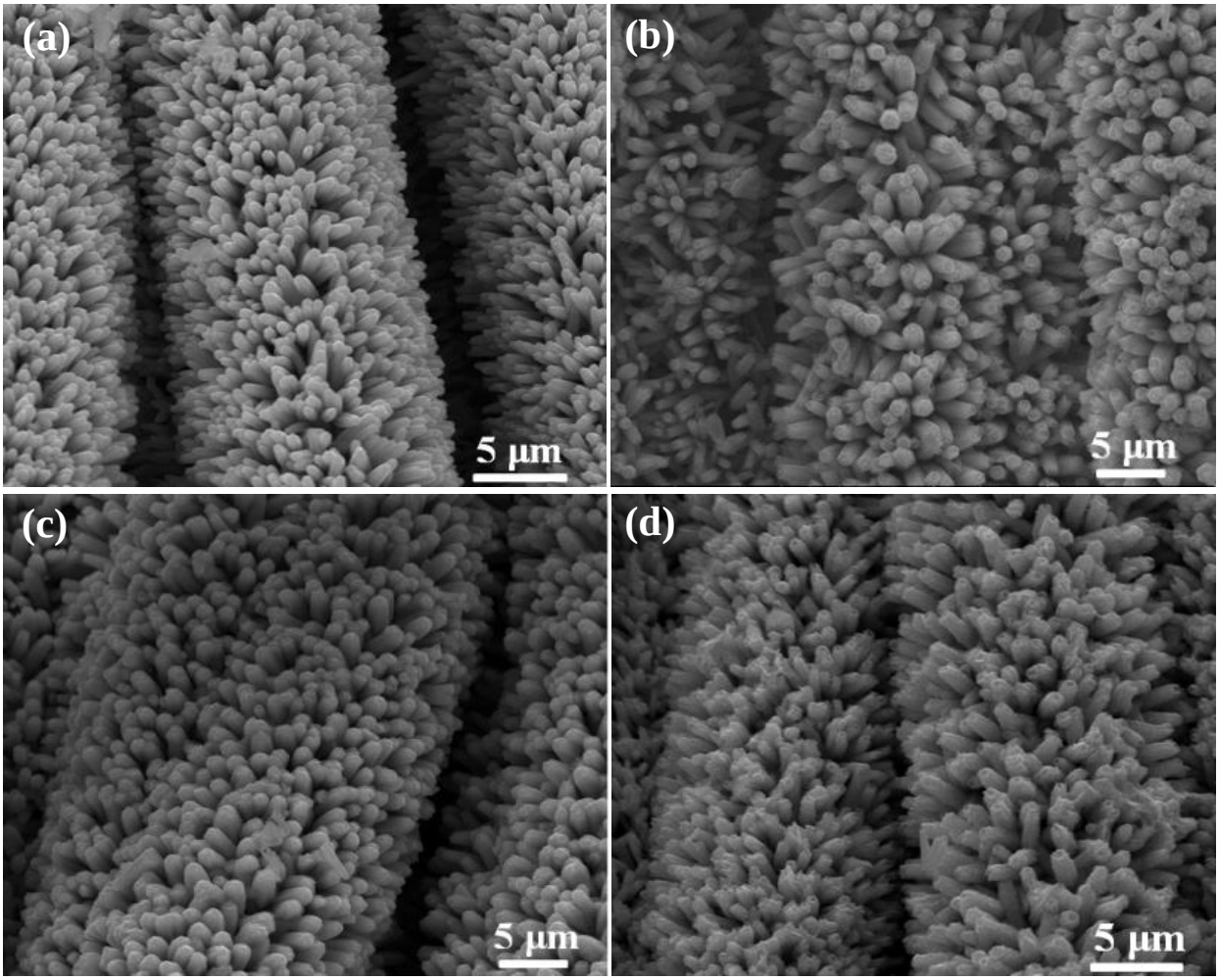

Figure S2. SEM images of various precursors: (a) ZnO MRAs/CFC, (b) ZnO@MnO_2MRAs/CFC, (c) ZnO@MnO_2@ZnOMRAs/CFC, and (d) ZnO@MnO_2@ZnO@ MnO_2MRAs/CFC.

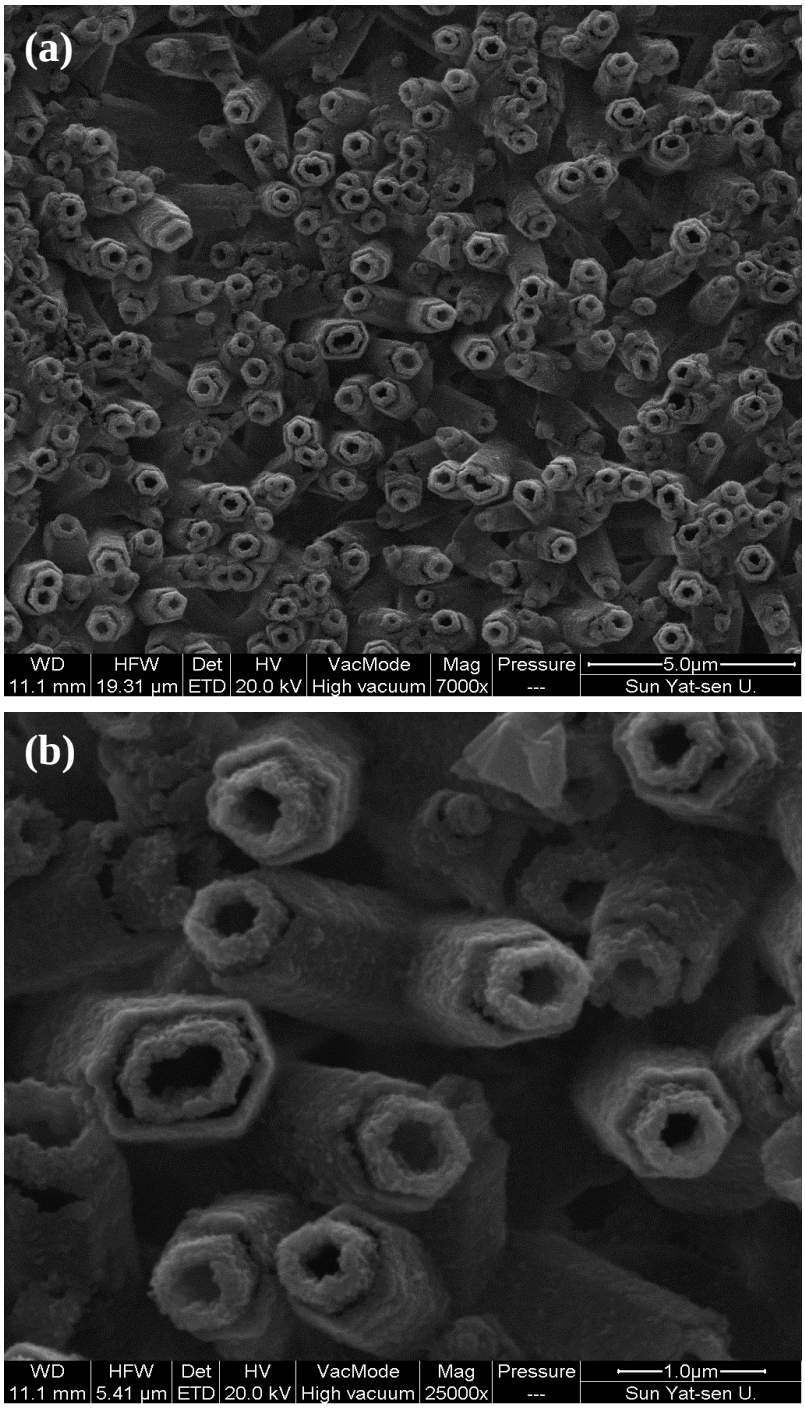

Figure S3. SEM images of the MnO_2 tube-in-tube arrays (TTAs) with different magnifications on Ti substrate.

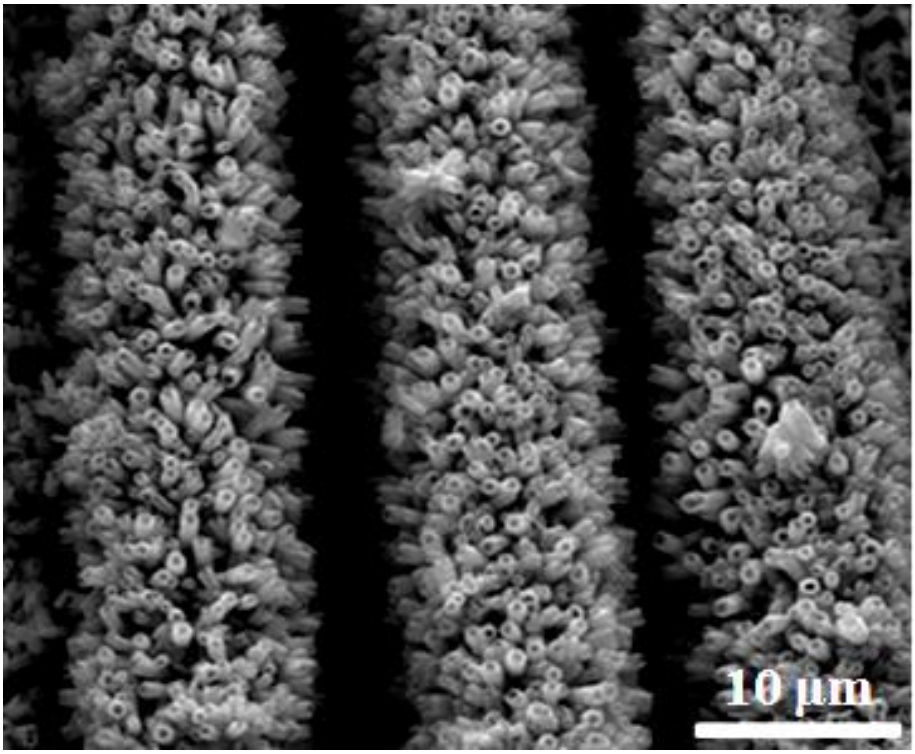

Figure S4. SEM image of MnO_2 STAs/CFC.

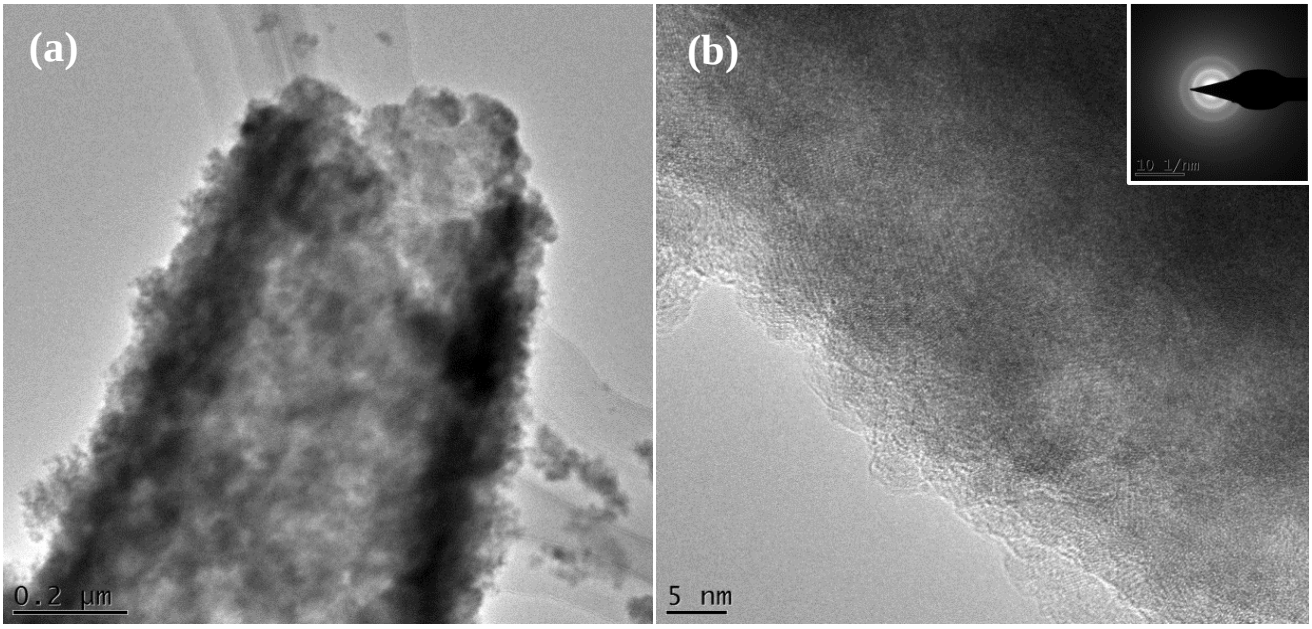

Figure S5. (a) TEM image, (b) HRTEM image and SAED (inset in (b)) of MnO_2 STAs.

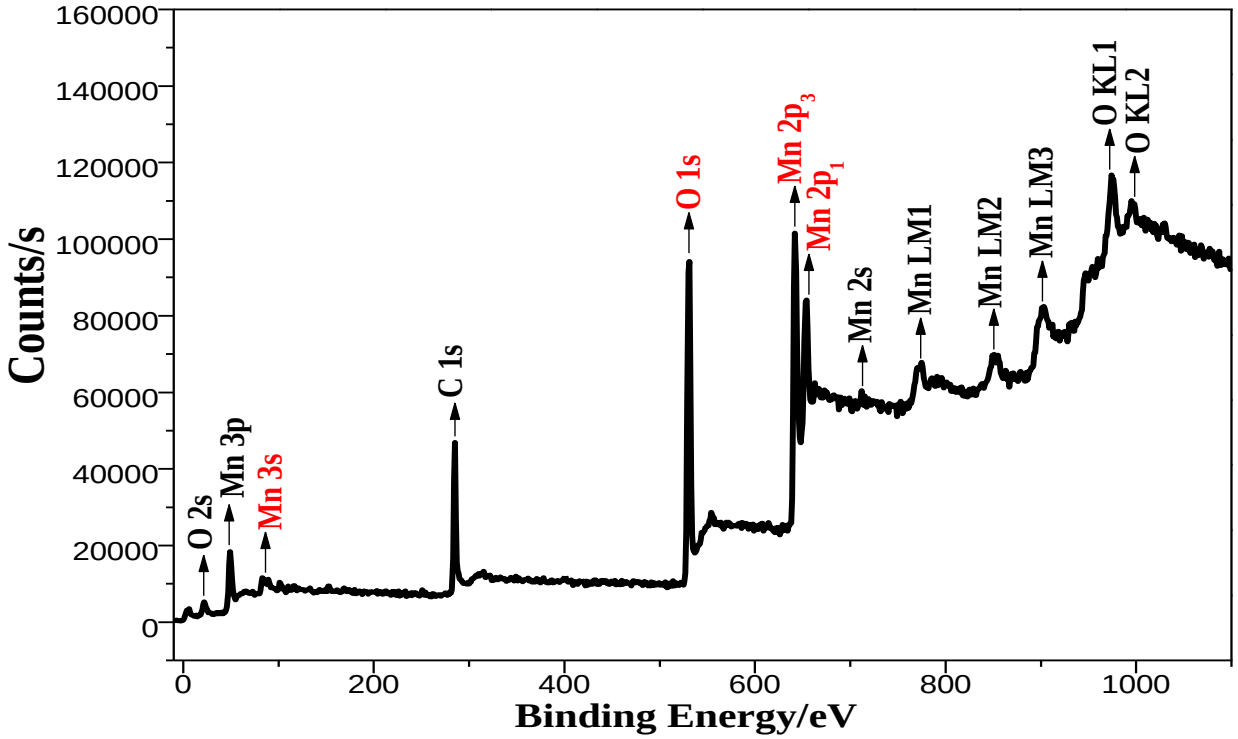

Figure S6. The XPS full spectrum of MnO_2TTAs/CFC.

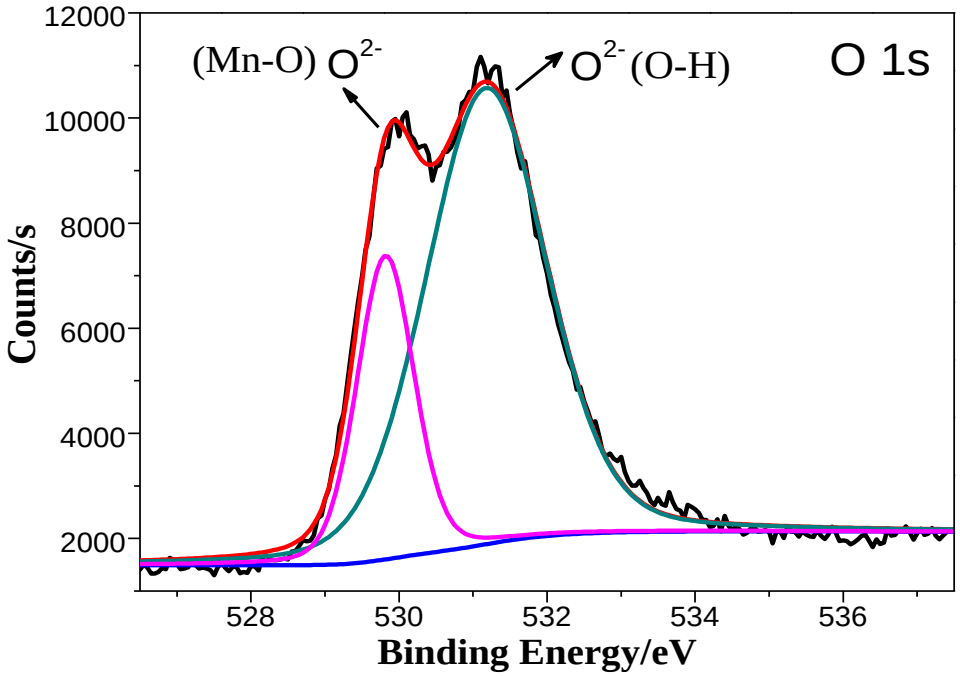

Figure S7. XPS spectrum of O_{1s} of the MnO_2 TTAs/CFC.

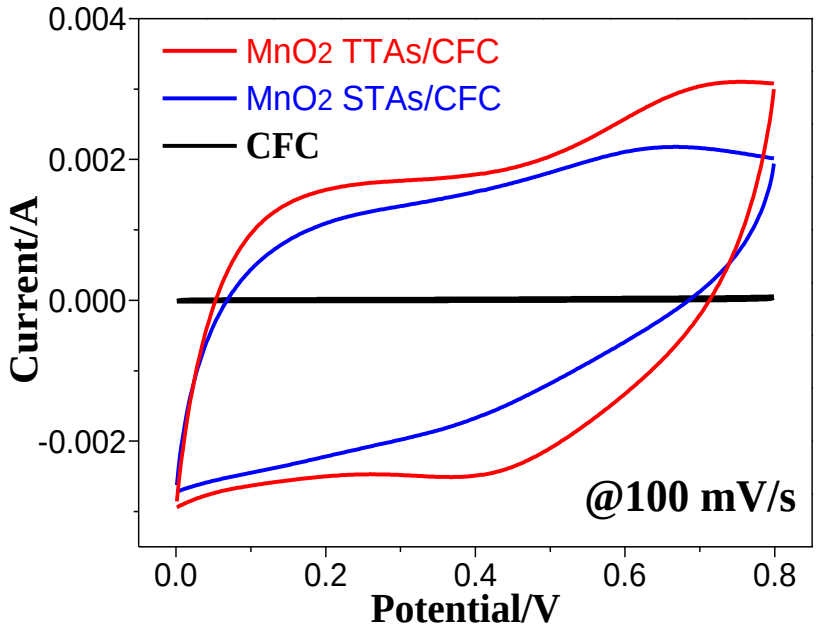

Figure S8. CVs of MnO_2 TTAs/CFC, MnO_2 STAs/CFC, and CFC at 100 mV/s.

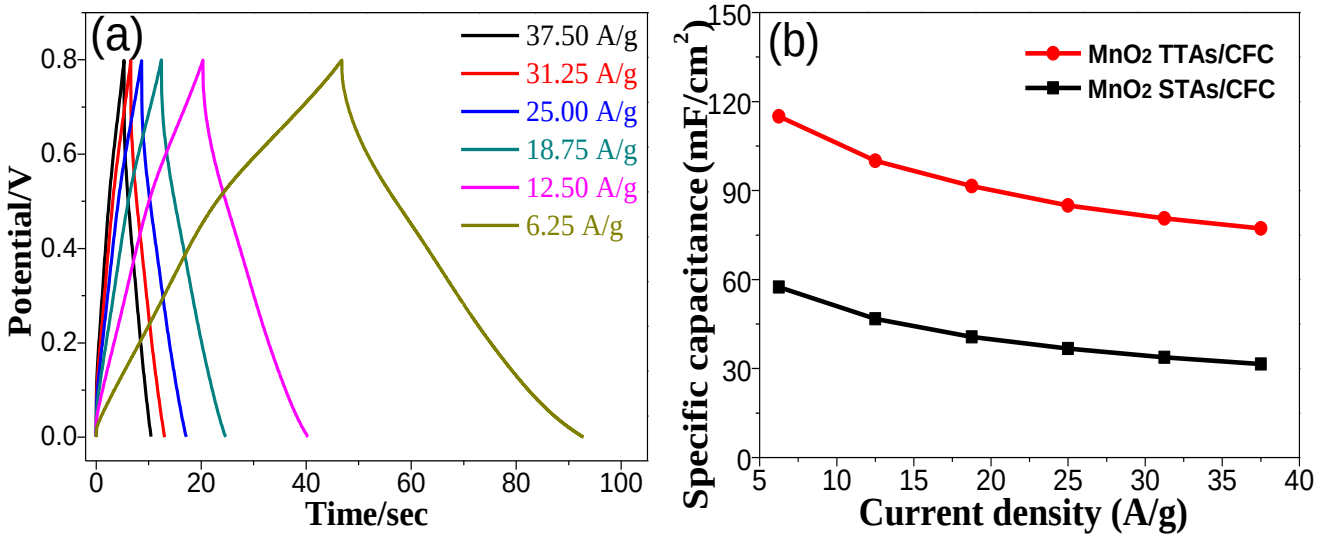

Figure S9. (a) GCD curves of MnO_2 TTAs/CFC at different current densities among 6.25~37.5 A/g. (b) The dependence of C_{sp} on current densities for MnO_2 TTAs/CFC among 6.25~37.5 A/g.

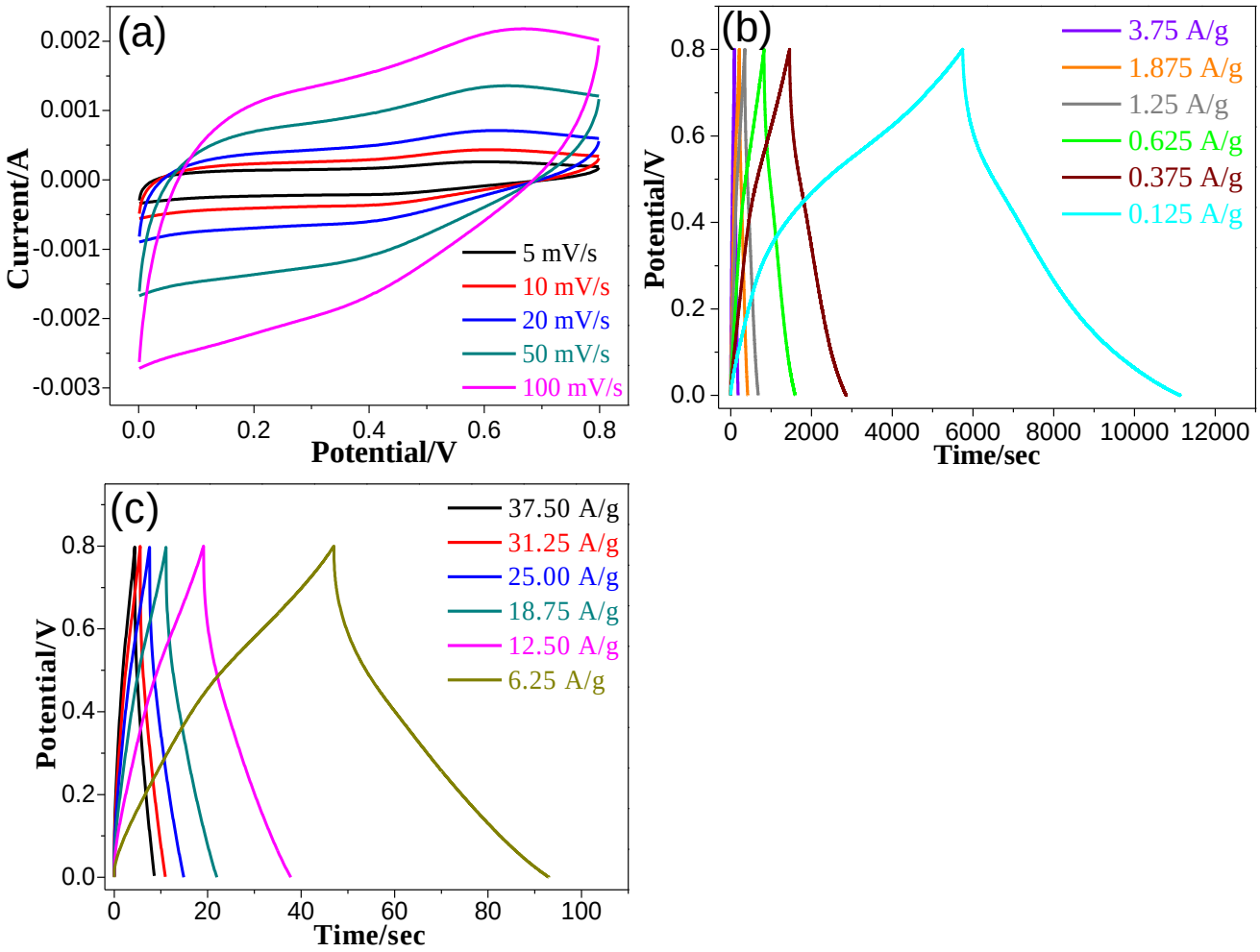

Figure S10. (a) CVs of MnO_2 STAs/CFC at different scan rates, (b-c) GCD curves of MnO_2 STAs/CFC at different current densities.

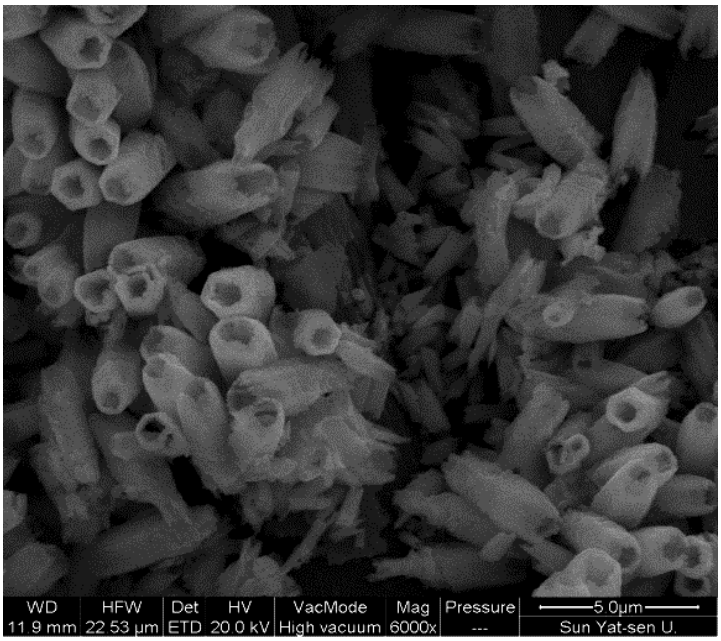

Figure S11. SEM image of MnO_2 STAs/CFC after 2000 cycles.

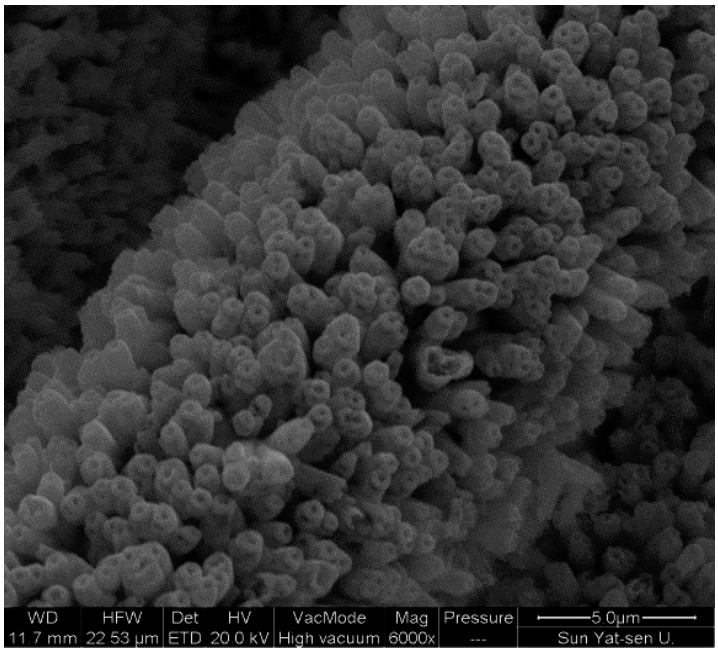

Figure S12.SEM image of MnO_2 TTAs/CFC after 2000 cycles.

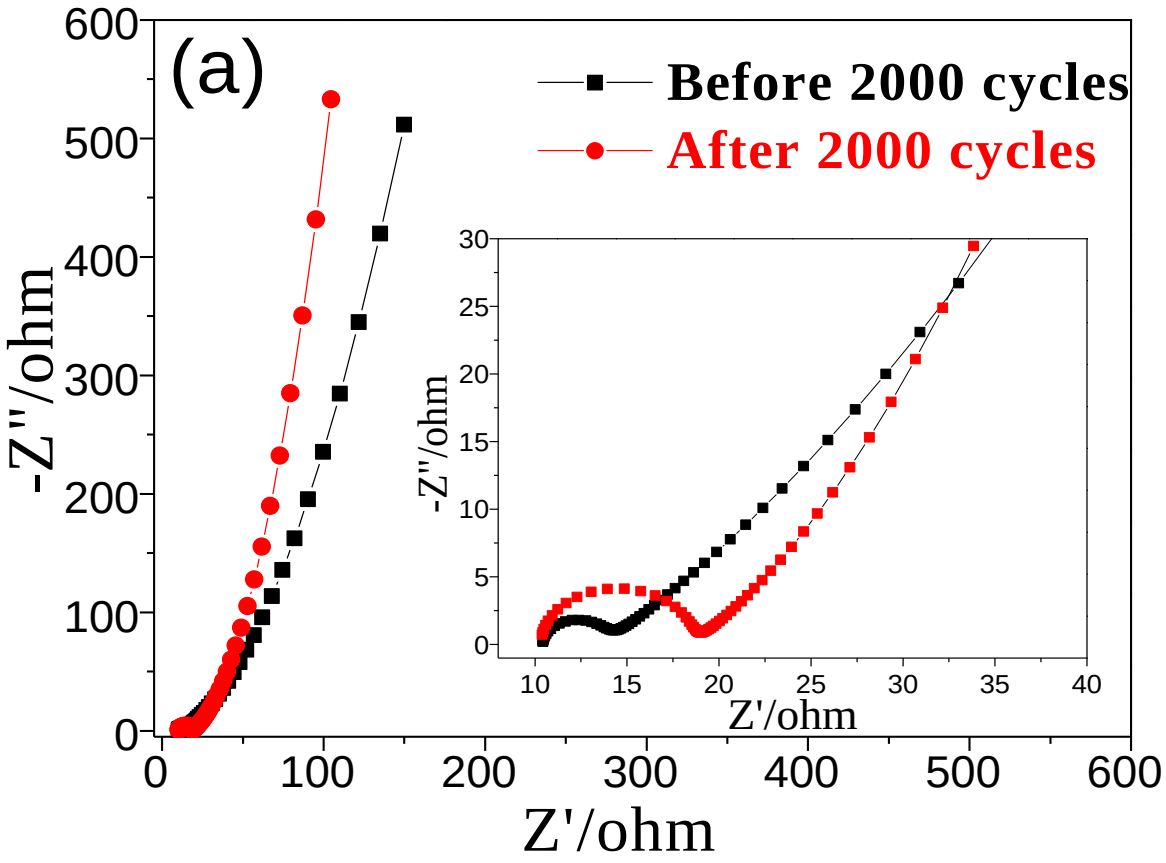

Figure S13. Nyquist plots of MnO_2 STAs/CFC before and after 2000 cycles.

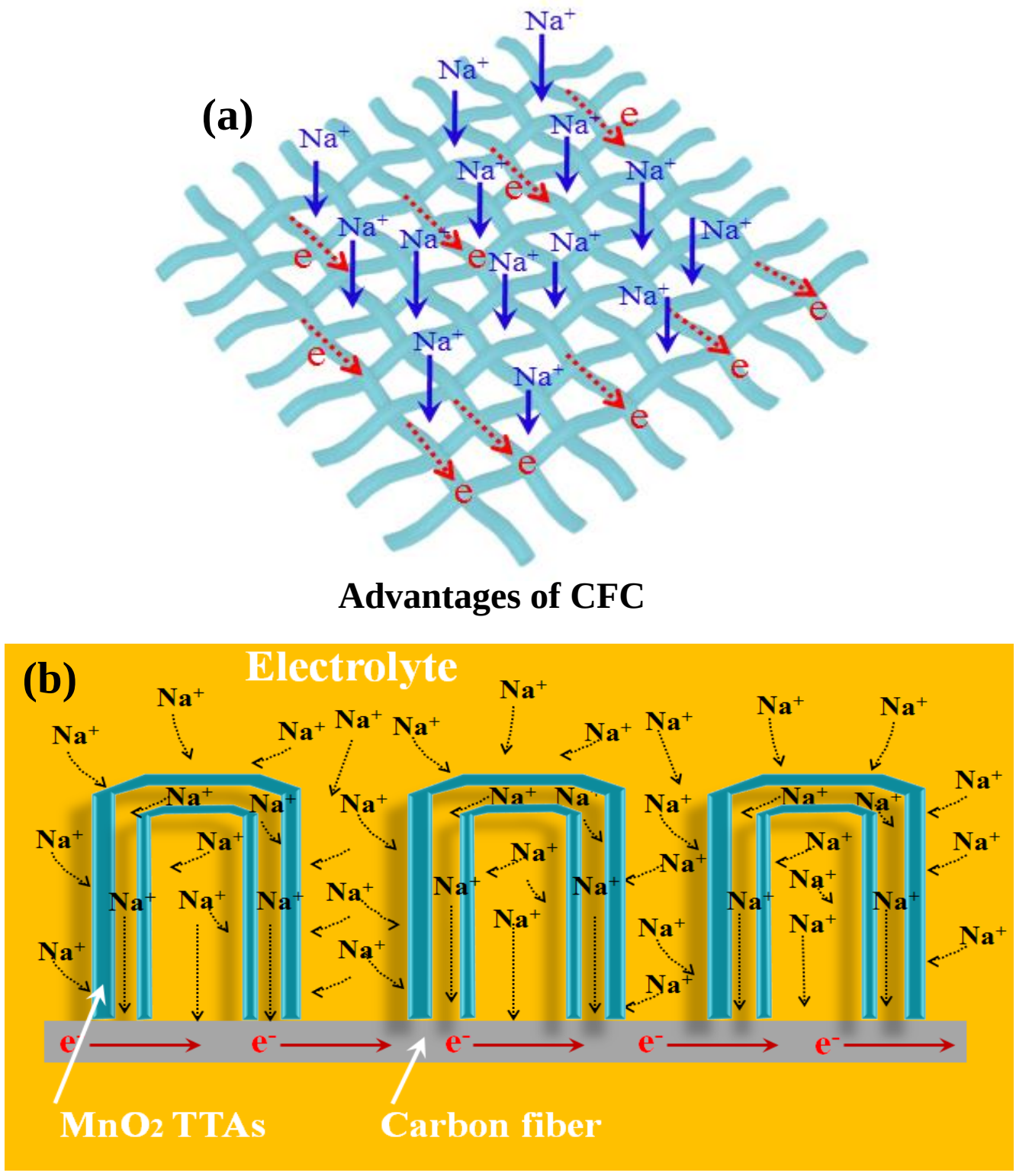

Figure S14. The fast ion and electron transmissions and high utilization rate in MnO_2 TTAs/CFC. (a) Schematic illustration for fast ion and electron transmissions in MnO_2TTAs/CFC electrode; (b) TTAs architecture provides "highways" for ions and high utilization for MnO_2TTAs/CFC electrode.

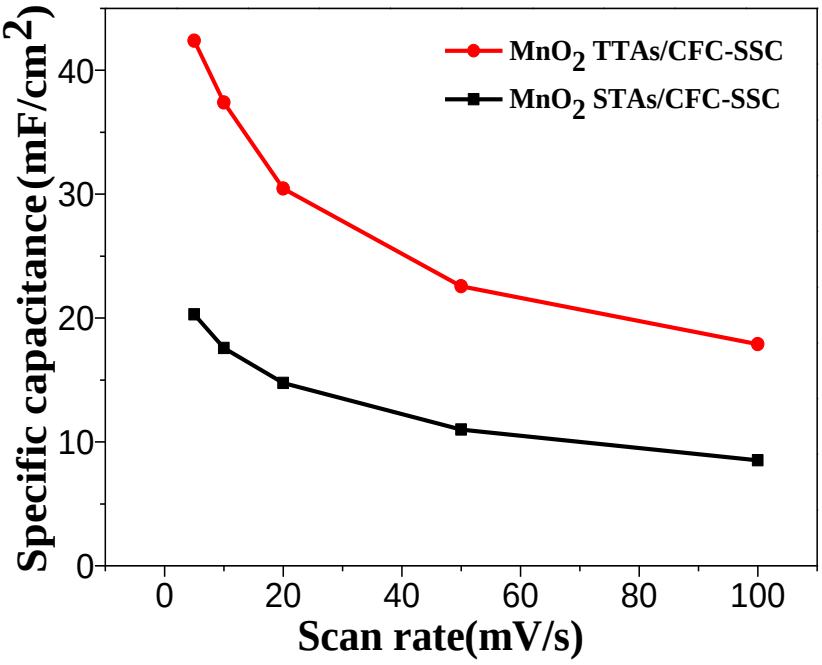

Figure S15. C_{sp} of MnO_2 TTAs/CFC-SSC and STAs/CFC-SSC as a function of scan rate.

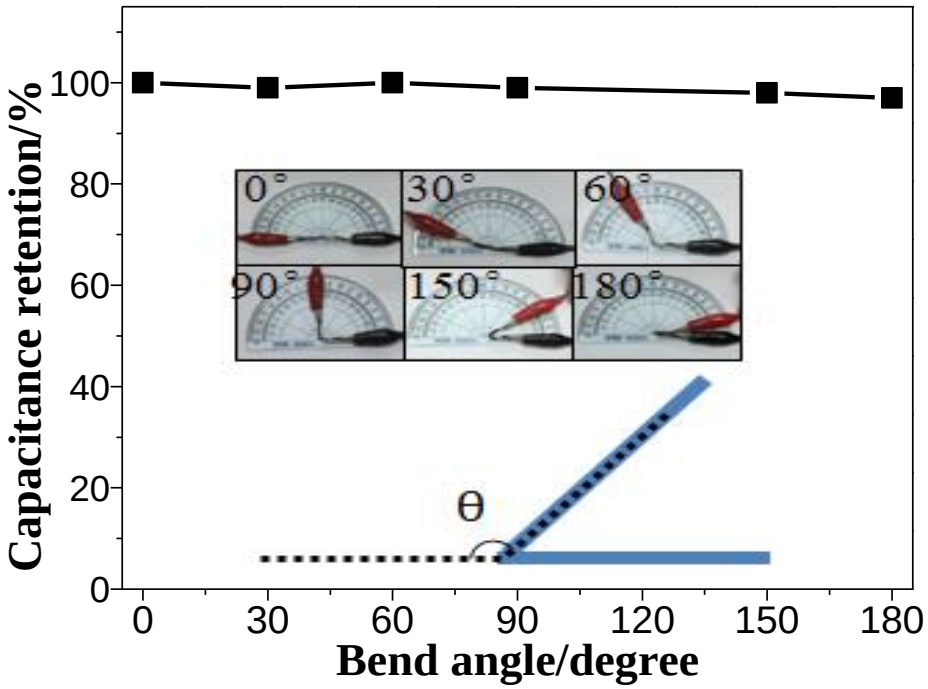

Figure S16. C_{sp} retention of MnO_2 TTAs/CFC-SSC device measured at different bend angles. Insets are the pictures of the device under different bend conditions and the schematic illustration of bend angle.

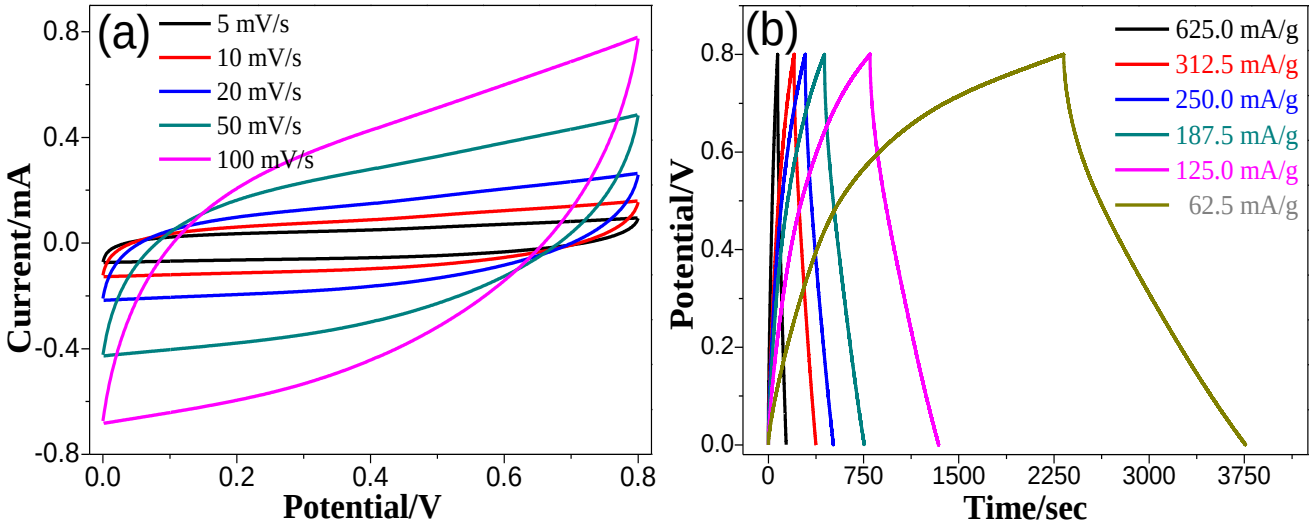

Figure S17. (a) CVs of MnO_2 STAs/CFC-SSC at different scan rates and (b) GCD curves of MnO_2 STAs/CFC-SSC at different current densities.

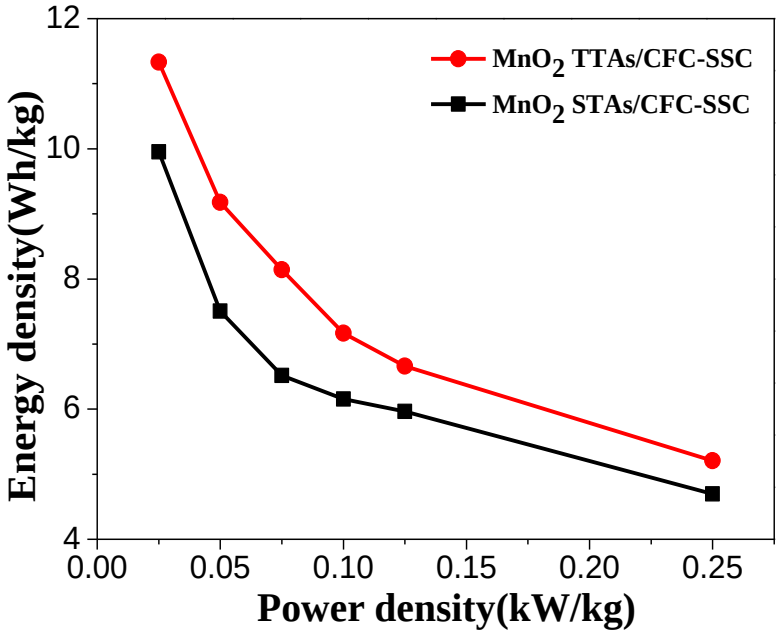

Figure S18. Ragone plots of MnO_2 TTAs/CFC-SC and MnO_2 STAs/CFC-SSC.